Applied Catalysis B: Environmental 253 (2019) 317–322

Contents lists available at ScienceDirect

Applied Catalysis B: Environmental

journal homepage: www.elsevier.com/locate/apcatb

Oxygen defect-ridden molybdenum oxide-coated carbon catalysts for Li-O_2 battery cathodes

Xuecheng Cao[a,b], Xiangjun Zheng[a,b], Zhihui Sun[a,b], Chao Jin[a,b], Jinghua Tian[a,b], Shaorui Sun[c,**], Ruizhi Yang[a,b,*]

[a] College of Energy, Soochow Institute for Energy and Materials InnovationS, Soochow University, Suzhou, Jiangsu 215006, China
[b] Key Laboratory of Advanced Carbon Materials and Wearable Energy Technologies of Jiangsu Province, Soochow University, Suzhou, Jiangsu 215006, China
[c] Beijing Key Laboratory for Green Catalysis and Separation, College of Environmental and Energy Engineering, Beijing University of Technology, Beijing, 100124, China

ARTICLE INFO

Keywords:
Oxygen defect
Molybdenum oxide
Carbon
Electrocatalysts
Li-O_2 batteries

ABSTRACT

The aprotic Li-O_2 batteries with high theoretical energy density hold great promise for long-range electric vehicles and grid energy storage system. However, the high over-potential, poor cycling stability and the side reactions associated with the carbon electrocatalysts at the cathode limit the practical application of Li-O_2 batteries. To address these challenges, in this work, oxygen defect-ridden molybdenum oxide (MoO_x) was coated on the surface of carbon nanotubes (CNTs) (denoted as MoO_x/CNT) by a facile solvothermal reaction for the first time. This MoO_x layer not only protects the CNTs catalysts from the side reactions but also promotes the reversible formation of Li_2O_2, resulting in low overpotential and excellent cycling stability of MoO_x/CNT cathode. A charging overpotential of only about 0.52 V and an enhanced stability of more than 210 cycles are obtained for the as-prepared MoO_x-coated CNT cathode. First-principles study by density functional theory (DFT) reveals that the stabilization of LiO_2 intermediates is enabled on oxygen-defected MoO_x during discharge process, leading to the formation of large sheet-like Li_2O_2 crystallites that are easy to be decomposed during charge process. This makes a crucial contribution to the enhanced electrochemical performance of MoO_x/CNT cathode.

1. Introduction

The success of long-range electric vehicles and grid energy storage system depends on the development of advanced battery technology. Compared to the current commercial Li-ion batteries (LIBs), rechargeable aprotic lithium-oxygen (Li-O_2) batteries have attracted worldwide attention because of their high energy density and environmental friendliness. The theoretical energy density of Li-O_2 batteries is 3500 Wh kg^{-1} [1–3], which is much higher than that of Li-ion batteries. The basic reaction in Li-O_2 batteries is $2Li^+ + O_2 \leftrightarrow Li_2O_2$. The effective reversible formation and decomposition of Li_2O_2, associated with the oxygen reduction reaction (ORR) and oxygen evolution reaction (OER) at the cathode, is the key to unlock the full potential of Li-O_2 batteries [4–8]. An efficient electrocatalyst with high stability is required for the reactions at cathode of Li-O_2 batteries. Most of current Li-O_2 cathodes employ carbon as the catalyst due to its large specific surface area, high electrical conductivity and abundant resources. However, it's proven that carbon would react with Li_2O_2 and also promote the decomposition of electrolytes, leading to the formation of byproducts, such as carbonate and carboxylate. The resulting passivated layer is difficult to be decomposed during charge process, resulting in high overpotential, poor cycling stability and low coulomb efficiency of Li-O_2 batteries [9–12]. To circumvent these problems, carbon-free cathodes, such as gold [13], Ru/ITO [14], TiC [15] and Ti_4O_7 [16], have been studied. However, the gravimetric capacities of these electrodes are low due to their high mass density. In this regard, the surface protection of carbon electrocatalysts at the cathode has been reported to be a viable option to achieve high electrochemical performance of Li-O_2 batteries.

Protective coatings of Al_2O_3 + Pd [17] and ZnO [18] applied on the surface of carbon electrode by atomic layer deposition have been reported. The protected layer on carbon could suppress the side reactions, resulting in decreased overpotential and enhanced cycling stability [17,18]. However, the involving of noble metal Pd remains an issue in the case of Al_2O_3 + Pd coating. In the latter case, Li_2O_2 was formed at the interface between ZnO and carbon during continuous cycling due to the insulating nature of ZnO and weak binding between ZnO and carbon. This leads to the detachment of ZnO coating and exposure of bare carbon electrode, consequently degrading the performance of Li-

* Corresponding author at: College of Energy, Soochow Institute for Energy and Materials InnovationS, Soochow University, Suzhou, Jiangsu 215006, China.
** Corresponding author.
E-mail addresses: sunsr@bjut.edu.cn (S. Sun), yangrz@suda.edu.cn (R. Yang).

https://doi.org/10.1016/j.apcatb.2019.04.077
Received 1 January 2019; Received in revised form 19 April 2019; Accepted 22 April 2019
Available online 24 April 2019
0926-3373/

O_2 batteries with extended cycles [18]. Therefore, the protection of carbon electrocatalysts at the cathode with an effective and facile coating strategy and new coating materials still remains a great challenge.

Herein, we have successfully coated oxygen defect-ridden MoO_x layer on the surface of carbon nanotubes (CNTs) by a facile solvothermal reaction. The X-ray diffraction and X-ray photoelectron spectroscopy analyses reveal that this MoO_x layer is amorphous and oxygen-defects rich. When employed as a cathode in Li-O_2 batteries, a charging overpotential of only about 0.52 V, a high specific capacity of 8250 mA h g^{-1} at 200 mA g^{-1} and an enhanced stability of more than 210 cycles are obtained for the as-prepared MoO_x-coated CNT (denoted as MoO_x/CNT). Density functional theory (DFT) studies elucidate the origin of the high performance of MoO_x/CNT electrocatalysts at the cathode of Li-O_2 batteries. This work provides an effective surface-coating strategy with oxygen defect-ridden MoO_x as coating materials for protecting carbon electrocatalysts at the cathode of Li-O_2 batteries.

2. Experimental section

2.1. Synthesis of oxygen defect-ridden MoO_x-coated CNT

The synthesis of oxygen defect-ridden MoO_x-coated CNT (MoO_x/CNT) was carried out by a facile solvothermal process. Firstly, 0.2 g of commercial CNT powder was dispersed in 30 mL of ethanol. Then, 0.27 g of $MoCl_5$ and 15 μL of water were added into the above solution. After stirring for about 20 min, the solution was transferred to a 50 mL Teflon-lined stainless autoclave. The mixture was heated to 180 ℃ and maintained for 3 h. After it was cooled down to room temperature, the products were collected by centrifugation and washed by ethanol and deionized water for at least three times and dried at 40 ℃ under vacuum.

2.2. Synthesis of MoO_3-coated CNT

The MoO_3-coated CNT (MoO_3/CNT) was obtained by heating the MoO_x/CNT in air at 300 ℃ for 2 h. The electrochemical performance of the cathode made by MoO_3/CNT was also evaluated to compare with that of MoO_x/CNT.

2.3. Physical characterization

The phase of the synthesized samples were studied by X-ray diffraction (XRD) on a Bede D1 X-ray diffractometer (U.K., Bede scientific Ltd.; Cu K α radiation, λ = 0.15418 nm; operated at 40 KV, 45 mA). The morphology and microstructure of the samples were investigated on a scanning electron microscope (SEM, FEI Quanta 200) and a transmission electron microscope (TEM, Tecnai F20, 200 kV). The binding environment of all the elements in samples was analyzed on a X-ray photoelectron spectroscopy spectrometer (XPS, VG ESCALAB MKII). The spectrum position of each element was calibrated using 284.5 eV as the line position of carbon, which was corrected for the background using the Shirley approach.

2.4. Electrochemical measurements

Coin-type cells were designed to investigate the discharge and charge capacity, rate capability and cyclability of Li-O_2 batteries. The coin cells consisted of a cathode, a lithium foil anode (φ15 mm) and a glass microfiber filter (Whatman, φ19 mm, Maidstone, UK) membrane soaked in an electrolyte consisting of 1 M Lithium bis(trifluoromethanesulfonyl)imide (LiTFSI) (99.99%; Sigma-Aldrich) in dimethyl sulfoxide (DMSO). The MoO_x/CNT (or MoO_3/CNT) were mixed with binder poly tetra fluoroethylene (PTFE) by a ratio of 9:1. The resulting paste was coated on the surface of a carbon paper (TGP-H-030, Torray). The mass loading of catalysts on each cathode was about 0.5 mg. All measurements were conducted in 1 atm high-pure dry O_2 (> 99.999%) to avoid any negative effects of humidity and CO_2. The specific capacity and current density were calculated according to the mass of MoO_x/CNT (or MoO_3/CNT). To study the discharged products and the corresponding morphological and structural changes after discharge and charge process, the cells were discharged or charged to the required stages, and then disassembled in a glove box filled with Ar (> 99.999%). The cathodes were washed by DMSO several times to remove the residual lithium salt before being tested for ex-situ SEM and XPS.

2.5. Computation methods

First-principles density function theory (DFT) with the VASP package was used in all the calculations [19]. The projected-augmented wave (PAW) method was applied to treat the ion-electron interactions [20,21]. The exchange-correlation energy of electrons was calculated in the generalized gradient approximation (GGA) scheme with the PBE functional parameterization [22]. The energy cut-off was 400 eV, and the energy criterion of the self-consistent convergence was placed as at 0.0001 eV $atom^{-1}$. For body phase calculation, the k point sampling in the first Brillouin zone is 5 × 2 × 5. Here the free energy difference (ΔG) is only considered as the total energy difference (ΔE), which could be got through DFT calculation. The MoO_3 (010) surface is constructed with six layers and 2 × 2 two dimensional supercell, and the vacuum layer is more than 15.0 Å. The k point sampling in the first Brillouin zone is set as 3 × 3 × 1. In the MoO_x, the ratio of Mo^{6+} : Mo^{4+} is determined as 3:1.

3. Results and discussion

The synthesis process of MoO_x-coated CNT (denoted as MoO_x/CNT) is illustrated in Fig. 1a. The protecting layer of MoO_x (32 wt.%, Fig. S1, Supporting Information) was coated on the surface of CNTs by a facile solvothermal reaction. The obtained MoO_x/CNT maintains 3D interconnected nanotubes network with void spaces as observed from the scanning electron microscopy (SEM) image (Fig. S2a in the Supporting Information), which is beneficial for the transport of O_2 and electrolyte as well as the storage of discharge products. Fig. S2b (Supporting Information) shows the X-ray diffraction (XRD) pattern of MoO_x/CNT. Two diffraction peaks at 25.9° and 43.1° can be assigned to the (002) and (101) planes of the CNTs, respectively. There are no obvious diffraction peaks of Mo or Mo oxides. As the obtained sample was further heated to 300 ℃ in air, monoclinic MoO_3 was formed as revealed from the XRD pattern in Fig. S3a (Supporting Information). Some large particles with size of several hundred nanometers exist in the sample due to the agglomeration of Mo oxides upon the high temperature treatment (Fig. S3b in the Supporting Information). The comparison between the SEM-EDS spectra of CNT, MoO_x/CNT and MoO_3/CNT shows the existence of Mo and O in the as-prepared MoO_x/CNT (Figs. S4–S6 in the Supporting Information). The results indicate that the MoO_x exists in the MoO_x/CNT and it is amorphous since no diffraction peaks of molybdenum oxides can be observed in the XRD pattern (Fig. S2b in the Supporting Information). The transmission electron microscopy (TEM) images of pristine CNT and MoO_x/CNT are shown in Fig. S7 (Supporting Information), Fig. 1b and c. A coating layer with a thickness of ~5 nm on the surface of CNT can be clearly observed (Fig. 1c). There are no lattice fringes in the coating layer, which reveals that the MoO_x is amorphous; this is consistent with the XRD analysis. The EDX linear scan results of individual MoO_x/CNT (Fig. S8 in the Supporting Information) demonstrate higher Mo intensity at the edge of CNT than that in the middle part, which suggests that the MoO_x is coated on the surface of CNT. The scanning transmission electron microscopy (STEM) image of MoO_x/CNT and the corresponding elemental mapping (Fig. S9 in the Supporting Information) showing the uniform distribution of Mo and O in carbon further proves the coating of MoO_x

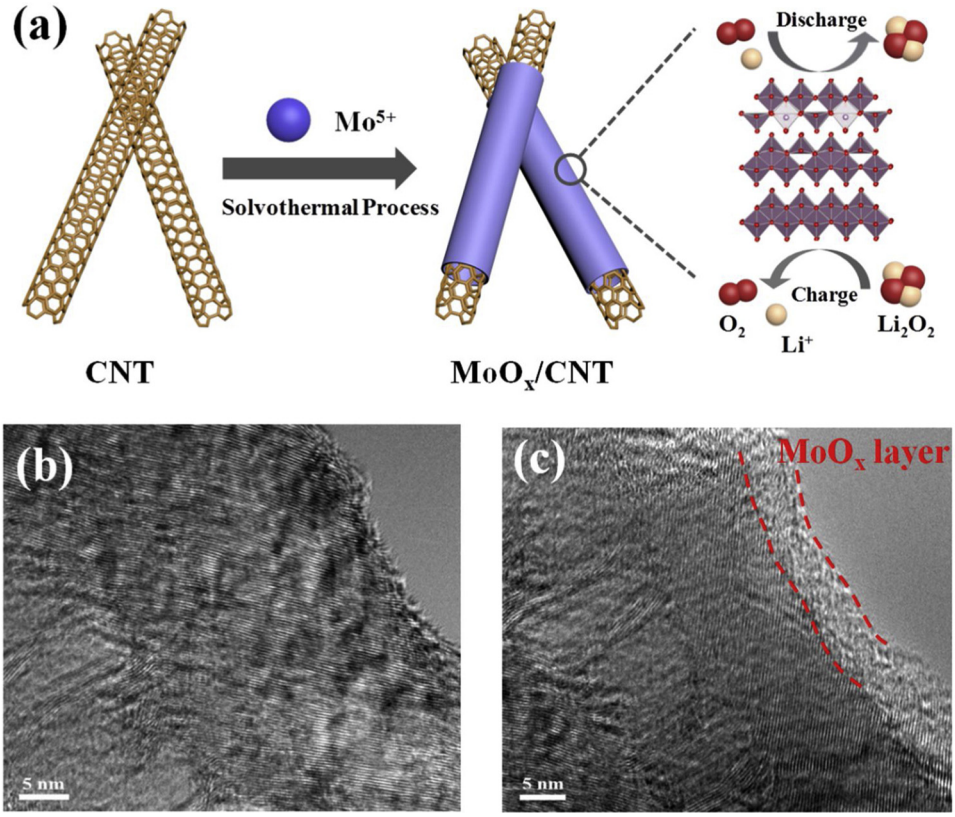

Fig. 1. (a) Schematic illustration of the synthesis of MoO_x-coated CNT (MoO_x/CNT). TEM images of (b) pristine CNT and (c) MoO_x/CNT.

on CNT.

In order to obtain the detailed cation oxidation state and the surface chemical composition of the MoO_x/CNT, X-ray photoelectron spectroscopy (XPS) measurements were conducted. In the high-resolution XPS spectrum of Mo $3d_{5/2}$ and Mo $3d_{3/2}$ in MoO_x/CNT (Fig. 2a), the two fitted peaks at 230.03 and 233.47 eV are attributed to Mo^{4+}, two peaks at 231.12 and 234.34 eV are ascribed to Mo^{5+}, and other two peaks at 232.45 and 235.57 eV can be assigned to Mo^{6+} [23–25]. These results indicate that the surface coating layer is a non-stoichiometric oxide corresponding to $Mo_{20}O_{49}$. While the fitted peaks of Mo 3d in MoO_3-coated CNT (MoO_3/CNT) (Fig. 2d) can only be ascribed to Mo^{6+} (232.1 and 235.3 eV), confirming the existence of MoO_3 [26]. The XPS spectrum of O 1s in MoO_x/CNT (Fig. 2b) shows high intensity of defected oxygen (532.5 eV) and chemisorbed oxygen (533.0 eV). While in the O 1s spectrum of MoO_3/CNT (Fig. 2e), the lattice oxygen (530.0 eV) is the dominant component. The results indicate that the surface of MoO_x/CNT is enriched with oxygen defects.

The C 1s spectra of MoO_x/CNT and MoO_3/CNT are shown in Fig. 2c

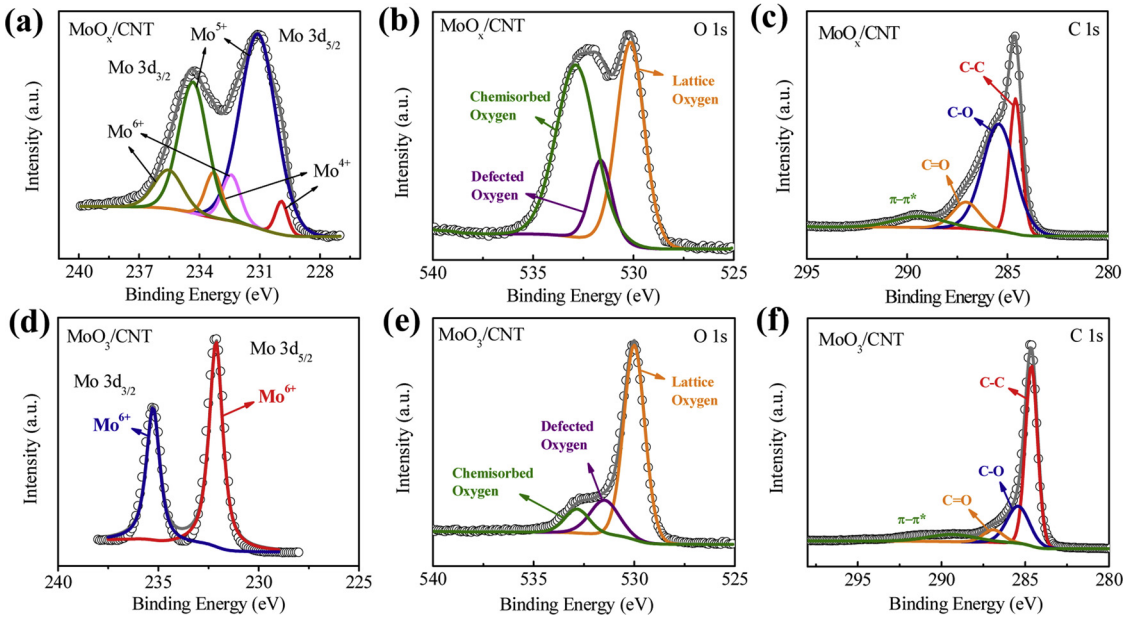

Fig. 2. High-resolution XPS spectra of Mo 3d (a), O1s (b) and C 1s (c) in MoO_x/CNT. High-resolution XPS spectra of Mo 3d (d), O1s (e) and C 1s (f) in MoO_3/CNT.

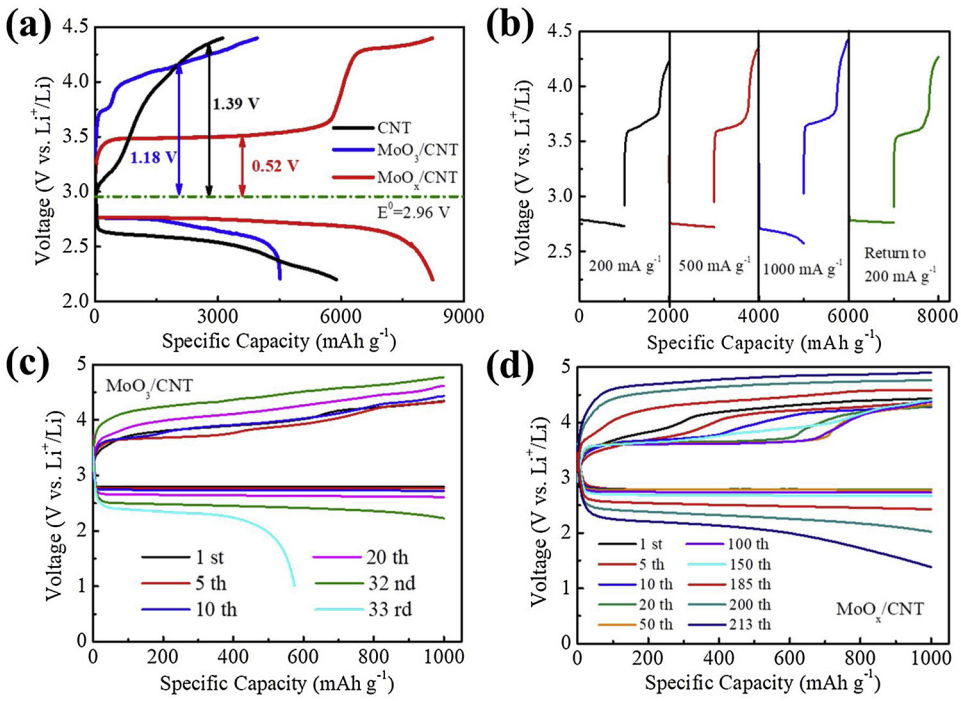

Fig. 3. (a) Voltage profiles of Li-O_2 batteries during galvanostatic discharge and charge with MoO_x/CNT, MoO_3/CNT and CNT cathodes. (b) Rate capability of Li-O_2 batteries with MoO_x/CNT cathode at different current densities. Cycling performance of (c) MoO_3/CNT and (d) MoO_x/CNT at a fixed specific capacity of 1000 mAh g^{-1}.

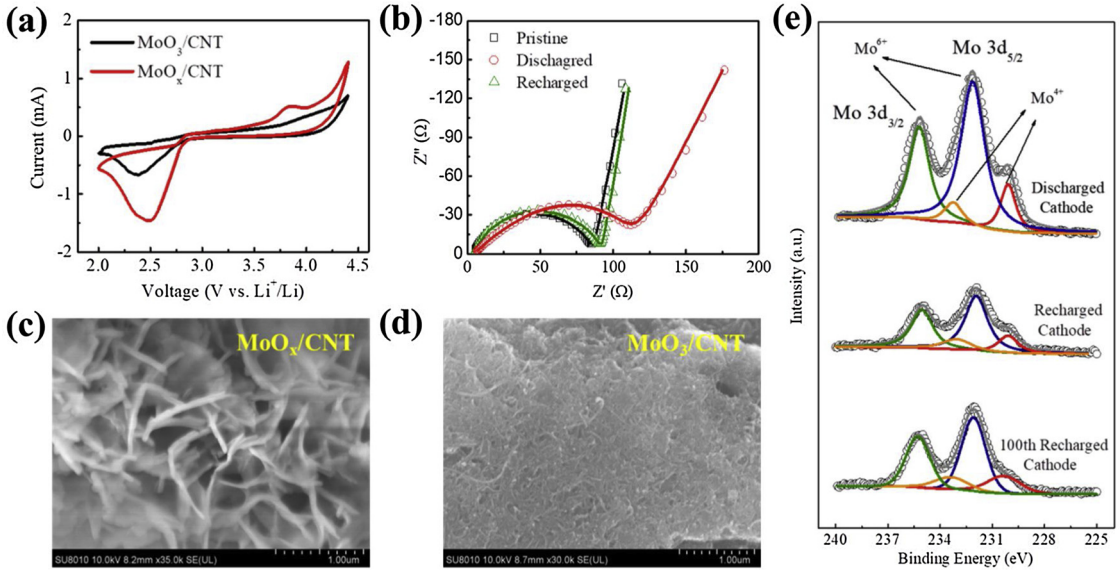

Fig. 4. (a) CV curves of Li-O_2 batteries with MoO_x/CNT cathode. (b) EIS of pristine, discharged and recharged Li-O_2 batteries with MoO_x/CNT cathode. (c) SEM image of discharged MoO_x/CNT cathode, the discharge product shows sheet-like morphology. (d) SEM image of discharged MoO_3/CNT cathode, the discharge product shows film-like morphology. (e) High-resolution XPS spectra of Mo 3d in the 1st discharged, 1st recharged and 100th recharged MoO_x/CNT cathode.

and f, respectively. The spectra can be fitted to C—C (284.6 eV), C—O (285.5 eV), C═O (287.1 eV) and π-π* (289.4 eV) [27]. The higher intensity of C—O bonding in MoO_x/CNT than that in MoO_3/CNT might result from the strong chemical coupling between MoO_x and CNT.

The electrochemical performance of MoO_x/CNT cathode was evaluated in Li-O_2 batteries. For comparison, the electrochemical performance of CNT and MoO_3/CNT cathodes was also tested under same conditions. The first discharge/charge profiles of pristine CNT, MoO_3/CNT and MoO_x/CNT cathodes at a current density of 100 mA g^{-1} are shown in Fig. 3a. The discharge capacity of MoO_x/CNT is about 8100 mAh g^{-1}, which is much higher than that of MoO_3/CNT (4500 mA h g^{-1}) and pristine CNT (5950 mA h g^{-1}). Notably, the charging overpotential of Li-O_2 batteries with MoO_x/CNT is only 0.52 V, which is much lower than that of MoO_3/CNT (1.18 V) and pristine CNT (1.39 V).

Fig. 3b displays the rate capability of MoO_x/CNT cathode at a limited specific capacity of 1000 mAh g^{-1}. At a current density of 200 mA g^{-1}, the charge voltage plateau of MoO_x/CNT is at ~3.50 V. It only increases slightly to ~3.63 V even at a high current density of 1000 mA g^{-1}. However, the charge voltage plateau of MoO_3/CNT cathode reaches 4.37 V as the current density increases to 1000 mA g^{-1} (Fig. S10 in the Supporting Information). The results reveal the superb rate capability of MoO_x/CNT. Fig. 3c and d show the cycling performance of MoO_3/CNT and MoO_x/CNT cathodes at a limited specific capacity of 1000 mAh g^{-1}, respectively. The MoO_3/CNT fails after only 33 cycles (Fig. 3c). In contrast, the MoO_x/CNT keeps continuous cycling for more than 210 cycles, displaying an enhanced cycling stability (Fig. 3d).

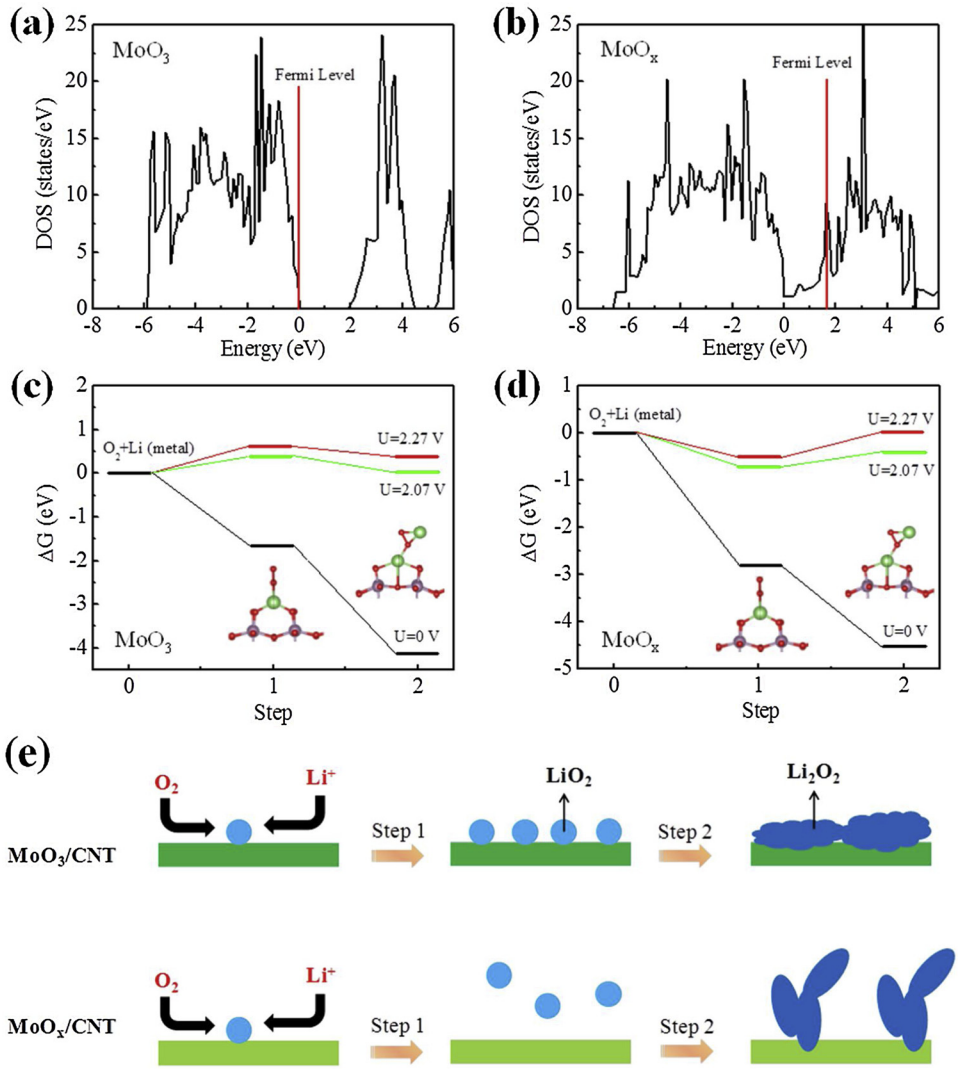

Fig. 5. The DOS of (a) MoO_3 and (b) MoO_x. Schematic free energy diagrams of oxygen reduction on (c) MoO_3 and (d) MoO_x surface. The reaction steps include the formation of LiO_2 (step 1) and the transformation of LiO_2 to Li_2O_2 (step 2). (e) Schematic illustration of discharge process of MoO_3/CNT and MoO_x/CNT cathode, respectively. The different adsorption energy of LiO_2 on MoO_3 and MoO_x surface induces the different morphology of Li_2O_2.

Cyclic voltammetry (CV) was applied to understand the electrochemical behavior of MoO_x/CNT cathode during discharge and charge process. As shown in Fig. 4a, the reduction peak potential of MoO_x/CNT is about 2.49 V (vs. Li^+/Li), which is much higher than that of MoO_3/CNT (2.36 V). This reduction peak corresponds to the formation of Li_2O_2 during discharge process. The oxidation peak at about 3.69–3.98 V for MoO_x/CNT represents the decomposition of Li_2O_2, which is lower than that for MoO_3/CNT (3.87–4.26 V). Meanwhile, the higher reduction/oxidation peak intensities can be observed on MoO_x/CNT. The results reveal higher electrocatalytic activity of MoO_x/CNT than that of MoO_3/CNT. Electrochemical impedance spectra (EIS) measurements were conducted to investigate the charge transfer resistance (R_{ct}) during discharge and recharge processes (Fig. 4b). The R_{ct} after discharge process increases remarkably due to the deposition of insulating discharge products Li_2O_2 on the cathode surface. After recharge, the R_{ct} decreases to a value similar to that of the pristine cathode, indicating the complete decomposition of Li_2O_2 and the recovery of MoO_x/CNT cathode. These results confirm the reversible discharge/recharge reactions of Li-O_2 battery with MoO_x/CNT cathode.

The morphology of discharged products on MoO_x/CNT cathode is shown in Fig. 4c. The formation of micrometer-sized sheet-like Li_2O_2 that is easy to be decomposed can be clearly observed on the discharged MoO_x/CNT cathode. In contrast, the SEM image in Fig. 4d shows that the film-like Li_2O_2 forms on MoO_3/CNT cathode. The characteristic peak of Li1s XPS spectra at a binding energy of about 55.5 eV (Fig. S11 in the Supporting Information) further proves that the Li_2O_2 is the desired dominant discharge product [28]. When the battery is charged to 4.4 V, the Li 1s peak disappears, which indicates the decomposition of Li_2O_2. The surface MoO_x layer after continuous discharge/recharge cycles was further studied with XPS. The Mo $3d_{5/2}$ and Mo $3d_{3/2}$ peaks corresponding to MoO_x still exist even after 100 continuous discharge/recharge cycles (Fig. 4e), suggesting that the surface MoO_x layer is stable during discharge and charge processes.

The density functional theory (DFT) analyses of MoO_x and MoO_3 were conducted to understand the effect of oxygen defect structure on the electrocatalytic activity of MoO_x. As shown in Fig. 5a, there is a band gap of about 1.5 eV in the Density of State (DOS) of α-MoO_3. In contrast, in the oxygen- defected MoO_x, there is no band gap and the Fermi level is just right across a peak of DOS (Fig. 5b), which implies that the electronic conductivity of the MoO_x is clearly higher than that of MoO_3. In a Li-O_2 battery, the formation of Li_2O_2 could be generally considered as the following two steps:

Step 1: $M\ (catalysts) + O_2 + Li^+ + e^- \rightarrow M\text{-}LiO_2$

Step 2: $M\text{-}LiO_2 + O_2 + Li^+ + e^- \rightarrow M\text{-}Li_2O_2$ or $2LiO_2 \rightarrow Li_2O_2 + O_2$

Here, in order to simplify the calculation, only one Li_2O_2 dimer is considered. On MoO_3 surface, the structures of LiO_2 and Li_2O_2 after optimization and the values of free energy change (ΔG) under different potentials (U) are presented in Fig. 5c. At U = 0 V, the absolute value of ΔG2 (2.47 eV) is larger than that of ΔG1(1.65 eV); and at the reversible potential (U = 2.07 V), ΔG1 is over 0 eV, which implies that LiO_2 is an unstable intermediate on MoO_3 surface and thus transforms to final product Li_2O_2 immediately via step 2. Therefore, the discharge products are amorphous. On MoO_x surface, the structures of LiO_2 and Li_2O_2 are shown in Fig. 5d. As shown in Fig. 5d, at U = 0 V, the absolute value of ΔG2 (1.72 eV) is obviously smaller than that of ΔG1 (2.80 eV). At the reversible potential (U = 2.27 V), ΔG1 is below 0 eV, which demonstrates that LiO_2 is the stable intermediate. The growth of Li_2O_2 follows the solvation-mediated pathway, which includes the diffusion of LiO_2 in electrolyte and disproportionation from LiO_2 to Li_2O_2 (Fig. 5e) [29]. In this case, the LiO_2 dissolved in electrolyte gradually deposits on the cathode surface, resulting in the formation of micrometer-sized Li_2O_2 sheets (Fig. 5e) [29]. According to Fig. S12 (Supporting Information), for the DOS of MoO_x, the peak at Fermi level is attributed to the Mo-$3d_{zx}$ state. After the LiO_2 is absorbed on the surface, the Mo-$3d_{zx}$ state could bond with O-p_x state, leading to the large absolute value of ΔG1 on MoO_x. Therefore, the LiO_2 could be produced on the MoO_x surface, which is consistent with the experimental results.

4. Conclusions

In summary, oxygen defect-ridden molybdenum oxide (MoO_x) was coated on the surface of carbon nanotubes (CNT) successfully by a facile solvothermal reaction. When applying the catalyst as an cathode for Li-O_2 batteries, it shows a charging overpotential of only about 0.52 V and an enhanced stability of more than 210 cycles. The MoO_x layer not only protects the CNTs from the side reactions but also promotes the reversible formation and decomposition of Li_2O_2, resulting in low overpotential and excellent cycling stability. The oxygen-defected MoO_x has higher electronic conductivity than MoO_3 as demonstrated by the DFT calculation. More importantly, the DFT studies reveal that this oxygen-defected structure facilitates the formation of stable LiO_2, resulting in the growth of large sized sheet-like Li_2O_2 that is easier to be decomposed. These findings indicate that the surface coating of carbon with oxygen defect-ridden MoO_x is effective in protecting carbon cathode of the Li-O_2 batteries. This work provides a new facile approach for designing electrodes to address the issues resulting from carbon catalysts for the application in energy storage and conversion technologies.

Acknowledgments

The authors acknowledge the financial support from the National Key Research and Development Program of China (2016YFB0100200), National Natural Science Foundation of China (Nos. 51572181), Natural Science Foundation of Jiangsu Province, China (BK20151226).

Appendix A. Supplementary data

Supplementary material related to this article can be found, in the online version, at doi:https://doi.org/10.1016/j.apcatb.2019.04.077.

References

[1] K.M. Abraham, Z. Jiang, J. Electrochem. Soc. 143 (1996) 1–5.
[2] P.G. Bruce, S.A. Freunberger, L.J. Hardwick, J.M. Tarascon, Nat. Mater. 11 (2012) 19–29.
[3] Z.L. Wang, D. Xu, J.J. Xu, X.B. Zhang, Chem. Soc. Rev. 43 (2014) 7746–7786.
[4] A.C. Luntz, B.D. McCloskey, Chem. Rev. 114 (2014) 11721–11750.
[5] J. Lu, L. Li, J.-B. Park, Y.-K. Sun, F. Wu, K. Amine, Chem. Rev. 114 (2014) 5611–5640.
[6] F.Y. Cheng, J. Chen, Chem. Soc. Rev. 41 (2012) 2172–2192.
[7] Z.L. Li, Z.C. Zhuang, F. Lv, H. Zhu, L. Zhou, M.C. Luo, J.X. Zhu, Z.Q. Lang, S.H. Feng, W. Chen, L.Q. Mai, S.J. Guo, Adv. Mater. 30 (2018) 1803220.
[8] Z.C. Zhuang, Y. Li, Z.L. Li, F. Lv, Z.Q. Lang, K.N. Zhao, L. Zhou, L. Moskaleva, S.J. Guo, L.Q. Mai, Angew. Chem. Int. Ed. 57 (2018) 496–500.
[9] Z.L. Wang, D. Xu, J.J. Xu, L.L. Zhang, X.B. Zhang, Adv. Funct. Mater. 22 (2012) 3699–3705.
[10] E. Yoo, H.S. Zhou, ACS Nano 5 (2011) 3020–3026.
[11] B.D. McCloskey, A. Speidel, R. Scheffler, D.C. Miller, J. Phys. Chem. Lett. 3 (2012) 997–1001.
[12] K.M.O. Thotiyl, S.A. Freunberger, Z.Q. Peng, P.G. Bruce, J. Am. Chem. Soc. 135 (2013) 494–500.
[13] Z.Q. Peng, S.A. Freunberger, Y.H. Chen, P.G. Bruce, Science 337 (2012) 563–566.
[14] F.J. Li, D.-M. Tang, Y. Chen, D. Golberg, H. Kitaura, T. Zhang, A. Yamada, H.S. Zhou, Nano Lett. 13 (2013) 4702–4707.
[15] M.M.O. Thotiyl, S.A. Freunberger, Z.Q. Peng, Y.H. Chen, Z. Liu, P.G. Bruce, Nat. Mater. 12 (2013) 1050–1056.
[16] D. Kundu, R. Black, E.J. Berq, L.F. Nazar, Energy Environ. Sci. 8 (2015) 1292–1298.
[17] J. Lu, Y. Lei, K.C. Lau, X.Y. Luo, P. Du, J.G. Wen, R.S. Assary, U. Das, D.J. Miller, J.W. Elam, H.M. Albishri, D.A. El-Hady, Y.K. Sun, L.A. Curtiss, K. Amine, Nat. Commun. 4 (2013) 2383–2391.
[18] Y.J. Bae, D.H. Ko, S.Y. Lee, H.D. Lim, Y.J. Kim, H.S. Shim, H.J. Park, Y.M. Ko, S.K. Park, H.J. Kown, H.J. Kim, H.T. Kim, Y.S. Min, D.M. Im, K.S. Kang, Adv. Energy Mater. (2018) 1702661.
[19] G. Kresse, J. Furthmuller, Comp. Mater. Sci. 6 (1996) 15–50.
[20] P.E. Blochl, Phys. Rev. B 50 (1994) 17953–17979.
[21] N.A.W. Holzwarth, G.E. Matthews, R.B. Dunning, A.R. Tackett, Y. Zeng, Phys. Rev. B 55 (1997) 2005–2017.
[22] J.P. Perdew, K. Burke, M. Ernzerhof, Phys. Rev. Lett. 77 (1996) 3865–3868.
[23] D. Kundu, R. Black, B. Adams, K. Harrison, K. Zavadil, L.F. Nazar, J. Phys. Chem. Lett. 6 (2015) 2252–2258.
[24] H. Yu, K.N. Dinh, Y.M. Sun, H.S. Fan, Y.H. Wang, Y. Jing, S.Z. Li, M. Srinivasan, Q.Y. Yan, Nanoscale 10 (2018) 14877–14884.
[25] Y. Yang, H.L. Fei, G.D. Ruan, C.S. Xiang, J.M. Tour, Adv. Mater. 26 (2014) 8163–8168.
[26] Z.Y. Yin, X. Zhang, Y.Q. Cai, J.Z. Chen, J.I. Wong, Y.Y. Tay, J.W. Chai, J. Wu, Z.Y. Zeng, B. Zheng, H.Y. Yang, H. Zhang, Angew. Chem. Int. Ed. 53 (2014) 12560–12565.
[27] X.J. Zheng, X.C. Cao, X.W. Li, J.H. Tian, C. Jin, R.Z. Yang, Nanoscale 9 (2017) 1059–1067.
[28] Q.C. Liu, J.J. Xu, X.B. Zhang, Nat. Commun. 6 (2015) 7892–7899.
[29] J.J. Xu, Z.W. Chang, Y. Wang, D.P. Liu, Y. Zhang, X.B. Zhang, Adv. Mater. 28 (2016) 9620–9628.